Singular Points of Polarizations in the Momentum Space of Photonic Crystal Slabs

Weimin Ye,[1,*] Yang Gao,[4] and Jianlong Liu[2,3,†]

[1]College of Advanced Interdisciplinary Studies, National University of Defense Technology, Changsha, 410073, China
[2]College of Physics, Harbin Institute of Technology, Harbin 150001, China
[3]College of Physics and Optoelectronic Engineering, Harbin Engineering University, Harbin 150001, China
[4]College of Electronic Engineering, Heilongjiang University, Harbin 150080, China

(Received 24 October 2019; accepted 13 March 2020; published 16 April 2020)

Bound states in the continuum (BICs), circularly polarized states (*C* points) and degenerate states are all of three types of singular points of polarization in the momentum space. For photonic crystal slabs (PhCSs) with linearly polarized far fields, BICs were found to be the centers of polarization vortices and attracted more attention in the previous studies. Here, we theoretically demonstrate that the far fields of PhCSs can exhibit remarkably diverse polarizations due to the robust existences of *C* points in the continuum. Only a pair of *C* points with identical handedness and opposite topological charge can be annihilated together. Continuously fine tuning of the structure parameters of PhCSs without breaking their symmetry, a pair of *C* points with identical topological charge and opposite handedness are able to merge into a BIC, then the BIC splits into *C* points again. Interestingly, a Dirac-degenerate BIC with one-half of topological charge is observed when two pairs of *C* points with identical topological charge from the upper and lower band, respectively, simultaneously merge at the Dirac-degenerate point. The law of topological charge conservation is verified to play an important role in the evolutions and interconversions between different types of polarization singularities. Our findings might shed light on the origin of singular points of polarization, could open a gateway towards the applications of them in the generation and manipulation of vector beams.

DOI: 10.1103/PhysRevLett.124.153904

Analogous to polarization singularities in real space of the monochromatic electromagnetic fields (vector fields) [1–4], singular points of polarizations in the momentum space are referred to as eigenmodes of optical systems with undefined polarization directions in the far fields. There are only three types of singular points of polarizations: *V* points (where the intensity of far field vanishes), *C* points (where the far field is pure circular polarization), and degenerate points at band degeneracies (where the far-field polarization is undetermined). Owing to the advantages in the designs, fabrications, and on-chip applications, Bloch leaky modes supported by photonic crystal slabs (PhCSs) [5,6] can present all types of singular points of polarizations in their momentum space, which has attracted considerable attention [7–19]. Worth noting that leaky modes of PhCSs at *V* points are lossless and cannot couple with free-space radiations, they are indeed the optical bound states in the continuum (BICs) with infinite lifetimes [7–11]. For linearly polarized far fields, BICs (*V* points in the momentum space) have been verified to be the momentum-space vortex centers exhibited by the polarization vectors [12–14]. This topological property ensures the robust existence of BICs [12] and opens new applications for BICs in the creation of vortex lasers [15] and ultrahigh-*Q* guided resonances [16]. At *C* points, PhCSs only couple with the circularly polarized free-space radiations with identical handedness. It leads to strong chiroptical effects and can be directly utilized to modulate the ellipticity of light. This phenomenon was verified by employing the PhCSs with a pair of *C* points spawning from an eliminated BIC at the Γ point [17]. Besides, optically pumped BIC lasers were realized in the square-lattice PhCSs with double-degenerate BICs at the Γ point [18].

In the previous studies, the frequencies of all reported BICs [7–16], *C* points [17], and degenerate points [18,19] in the momentum space of PhCSs were below the diffraction limit. That is, only the zero-order diffraction of far fields was the propagating wave in free space. These singular points of polarizations [7–19] could not arrive at the boundary of the first Brillouin zone (FBZ) before they became guided modes. It is due to the fact that for any leaky mode of PhCSs on the boundary of FBZ, at least the 0th- and 1st (or -1st) -order diffractions of them are free-space radiations. Although the occurrence of more than one order diffractions could bring more restrictions on constructing the BICs, the interferences among them provide a degree of freedom to efficiently modulate the far-field polarization states of PhCSs beyond the diffraction limit. It is, therefore, expected that singular points of polarizations near the boundary of FBZ could exhibit a different topological nature from BICs below the diffraction limit [12].

In this Letter, focusing on the polarization singularities near the corner of FBZ, we study Dirac-degenerate points and BICs at K (K-point BICs) and *C* points supported by

the honeycomb-lattice PhCSs [20–22]. They are a direct analog to graphene and could introduce two degrees of freedom, pseudospins, and valleys to the photons, which are widely used in topological photonics [23]. Distinct from the linearly polarized far fields [9,12–16] and C points achieved by breaking the in-plane inversion symmetry of the PhCSs [17], we theoretically demonstrate that C points can emerge near K-point BICs and Dirac-degenerate points of PhCSs with 180° rotational symmetry around the z axis (the in-plane inversion symmetry) and time-reversal symmetries. As a result, far fields of the PhCSs exhibit remarkable polarization diversity. Circular polarizations, linear, and elliptical polarizations with variant orientations and ellipticities could appear near the K point. Continuously varying the geometric parameters of PhCSs without breaking their spatial symmetry, the appearance and disappearance of K-point BICs (the Dirac-degenerate BICs) are found to be accompanied by merging and generating one (two) pair(s) of C points, respectively. Thus, we propose to use the winding numbers of the trajectories of far-field polarization states on the Poincaré sphere around the S_3 axis to generally define the topological charges carried by the polarization singularities. The conservation law of topological charges carried by all singular points provides an intuitive understanding of the robust existence of C points in the continuum (above the light line) and the interconversions of different types of polarization singularities.

Figure 1(a) shows our considered 2D PhCS composed of a honeycomb array (a lattice constant a) of cylindrical holes (identical diameter D) etched in a free-standing dielectric slab (a thickness h and a refractive index $n = 2.02$ corresponding to Si_3N_4 [9]). Because of the z- and y-mirror symmetry (invariance under the operation σ_z changing z to $-z$ and σ_y changing y to $-y$), all eigenmodes of the

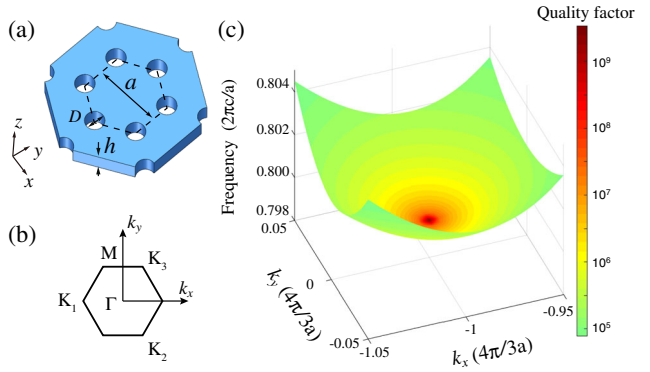

FIG. 1. Photonic crystal slab (PhCS) supporting a BIC at the K point. (a) Schematic illustration of the PhCS with a honeycomb array of cylindrical holes etched in a free-standing dielectric slab. (b) The first Brillouin zone in the momentum space of the honeycomb lattice with positions of $K_1 = -K\boldsymbol{e}_x$, $K = 4\pi/(3a)$. (c) Band structure of the PhCSs with (D, h) equal to ($0.3a$, $0.9074a$) near K_1 point. The color hues represent the quality factors (Q values) of the eigenmodes, which becomes infinite at the K_1 point.

PhCS could be divided into TM-like (defined by $\sigma_z = -1$) and TE-like ($\sigma_z = 1$) modes. The eigenmodes with the y component of the Bloch wave vector k_y equal to zero could be further divided into even (defined by $\sigma_y = 1$ in the Letter) and odd ($\sigma_y = -1$) modes [6]. Figure 1(b) depicts the FBZ of a honeycomb lattice. At its corners, three K points, denoted by K_j, $j = 1, 2, 3$, are equivalent to each other. For leaky modes at the K_1 point, the 0th-order and the two 1st-order diffractions with in-plane wave vectors equal to K_2 and K_3, respectively, are three propagating waves in free space, which provides six leakage channels. Because of C_{3V} symmetry of the PhCSs at K points, the coefficients of the three diffractions are not independent. Only one (two) leakage channel superposed by them is (are) symmetry compatible with the non-(Dirac-)degenerate leaky modes at K point. For example, the electric field of a single leakage channel compatible with a nondegenerate odd BIC at the K_1 point is given by $\boldsymbol{E}(\sigma_y = -1) = \boldsymbol{E}^{(\mathrm{TE})}_{K_1} + \boldsymbol{E}^{(\mathrm{TE})}_{K_2} + \boldsymbol{E}^{(\mathrm{TE})}_{K_3}$ ($\boldsymbol{E}^{(\mathrm{TE})}_{K_j}$ denotes the electric-field of a TE polarized plane wave with in-plane wave vector equal to K_j). Thus, none of the K-point BICs is a symmetry-protected BIC, which is different from Γ-point BICs [12,17]. By tuning geometric parameters, the PhCSs with (D, h) equal to ($0.3a$, $0.9074a$) is found to support a nondegenerate TE-like odd BIC at the K_1 point with a real normalized frequency $\omega a/2\pi c$ equal to 0.7998, which is located at the bottom of the band [Fig. 1(c)] (for the detailed band structures see Fig. s1 in Supplemental Material, note 1 [24]).

To look into the topological natures of the BIC, we examine the distributions of the far-field polarization states of the eigenmodes supported by the PhCSs in the vicinity of K_1 point [Fig. 2(a)] (For details of the method used to obtain the polarization states, see the Supplemental Material, note 2 [24]). Compatible with the odd symmetry of the BIC, the far fields of the eigenmodes with k_y equal to zero are TE polarizations (shown as a short line in the y direction). Interestingly, a pair of C points with the different handedness shown as the red and blue disc (corresponding to right- and left-handed circular polarizations, respectively) appear at (k_x, k_y) equal to ($-1.022K$, $-0.032K$) and ($-1.022K$, $0.032K$), respectively. When the handedness and the in-plane wave vector of the circularly polarized incident light match those of the C point, the reflectance spectrum of the PhCS exhibits a Fano line-shape curve with the resonant frequency approximately equal to that of the eigenmode at the C point. Utilizing a simplified scattering-matrix model [25] to study the couplings between fields inside the PhCS and the free-space leakages, we prove that both the C points and the K-point BIC are achieved by the interferences among multiple radiation channels (for details, see the Supplemental Material, note 3 [24]). Note that there is an L-line [2–4], where the far fields are linear polarizations, along the boundary between the

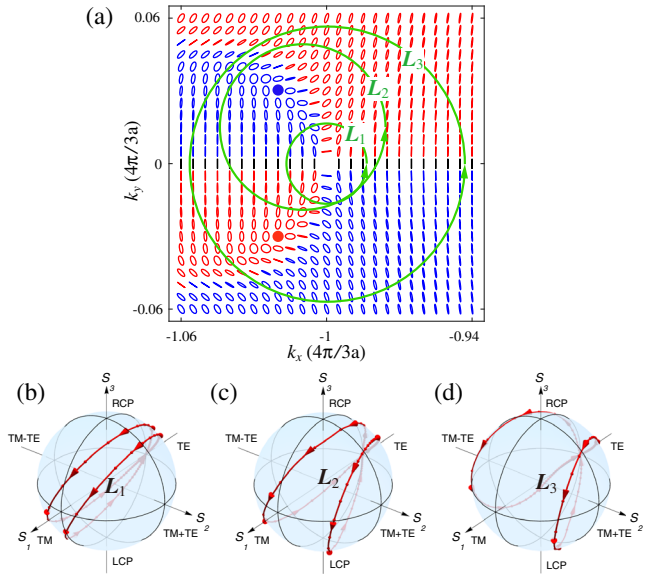

FIG. 2. Far-field polarization states of the PhCS supporting both BIC and C points in the momentum space. (a) Distribution of far-field polarization states of the PhCS near the K_1-point BIC [Fig. 1(c)]. The red (blue) ellipse denotes the right (left)-handed elliptic polarizations with different orientation angles. The red (blue) disc denotes the right (left)-handed C point. (b)–(d) Trajectories of far-field polarization states on the shell of the Poincaré sphere when Bloch wave vectors moving along the anticlockwise circles denoted by L_1 (b), L_2 (c), L_3 (d) shown in (a), respectively.

right- and left-handed ellipses. The predominant component of the electric field on the L line is TM polarization (shown as a short line in the x direction). The point of intersection between the L line and the line $k_y = 0$ in the momentum space is just the K_1 point (for details, see Fig. s4 in the Supplemental Material, Note 4 [24]). Owing to the y-mirror symmetry of the PhCS, the polarization direction of the far field at the K_1 point is undefined. Thus, the nondegenerate eigenmode at the K_1 point is a BIC with an infinite quality factor (Q value) [12]. The diverse far-field polarization states including linear, circular, and elliptical polarizations with different orientations cannot be simply described by a polarization vortex.

Here, we map the varying far-field polarization states on the shell of the Poincaré sphere, when Bloch wave vector $\boldsymbol{k}$ moves along an anticlockwise closed loop L enclosing singular points of polarizations in the momentum space. For a far-field polarization state with an orientation angle $\psi(\boldsymbol{k})$ and ellipticity angle $\chi(\boldsymbol{k})$, the longitude $\varphi(\boldsymbol{k})$ and the latitude $\theta(\boldsymbol{k})$ of its corresponding point on the shell of the Poincaré sphere are equal to 2ψ and 2χ, respectively. Similar to the C point located at the north and south poles with undefined longitude or orientation angle, the longitudes of the BIC and degenerate points (not shown on the shell of Poincaré sphere) are undefined. Thus, limited to the closed loop L enclosing only one BIC (C point or degenerate point on one of the degenerate bands), the topological charge q_B (q_C or q_D) carried by the BIC (C point or the degenerate point) can be defined as half of the winding number n_w (an integer) of the corresponding closed trajectory $G(L)$ around the S_3 axis on the shell of the Poincaré sphere. That is,

$$q_{B(C,D)} = \frac{1}{2\pi}\oint_L d\psi = \frac{1}{4\pi}\oint_{G(L)} d\varphi = \frac{n_w}{2}. \qquad (1)$$

Meanwhile, the winding number n_w of the closed trajectory G is double of the sum of topological charges carried by all polarization singularities enclosed within the corresponding closed loop L in the momentum space. The topological charge defined in Eq. (1) is consistent with that of the C and V points in real space [3,4]. When the far field is linearly polarized, the topological charge is just the winding number of the polarization vortex [12].

Three anticlockwise circles, denoted by L_1, L_2, L_3 in Fig. 2(a), enclosing the BIC with the radii $R_{\boldsymbol{k}}$ equal to $0.016K$, $0.033K$, $0.056K$ and the centers (k_x, k_y) equal to $(-K, 0)$, $(-1.01K, 0.015K)$, $(-K, 0)$, respectively, are selected to map the far-field polarization states on them to the shell of the Poincaré sphere. Figures 2(b)–2(d) show that the winding numbers of the three closed trajectories corresponding to circles L_1, L_2, and L_3 are equal to -2, -1, and 0, respectively. Since the amount of C points enclosed by circles L_1, L_2, and L_3 is 0, 1, and 2, the topological charge [Eq. (1)] carried by the BIC and the C point is -1 and $1/2$, respectively. [For the projected trajectories (letting $S_3 = 0$) of the three-dimensional trajectories in Figs. 2(b)–2(d) on the S_1-S_2 plane, see Figs. s5 in Supplemental Material, Note 5 [24]]. The conserved sum of the topological charges including the pair of C points and the BIC in the momentum space shown in Fig. 2(a) is zero, which plays an important role in their generations, evolutions, and annihilations.

To see the behaviors of these singularities in the momentum space, we slightly change the diameter D of the cylindrical holes etched in the PhCS [Fig. 1(a)] without breaking its symmetry. Noting that there are usually six (three) independent leakage channels in free space for leaky modes with Bloch wave vectors (along the ΓK direction or on the boundary of FBZ) close to the K point, the increased amount of leakage channels destroys the robustness of K-point BICs under small changes of geometric parameters of PhCSs. Without violating the conservation law of topological charges, the K-point BIC [in Fig. 2(a) with a topological charge of -1] should spawn two C points. Figure 3(a) exhibits that the K-point BIC just emerges at the point of intersection between the trajectories of a pair of C points [denoted by $-$R1/ $-$ L1 in Fig. 3(a) with opposite handedness and identical topological charges of $-1/2$]. When D is relatively small, this pair of C points locate inside the FBZ and close to the K_1 point. With the continuous increment of D, the pair of C points move

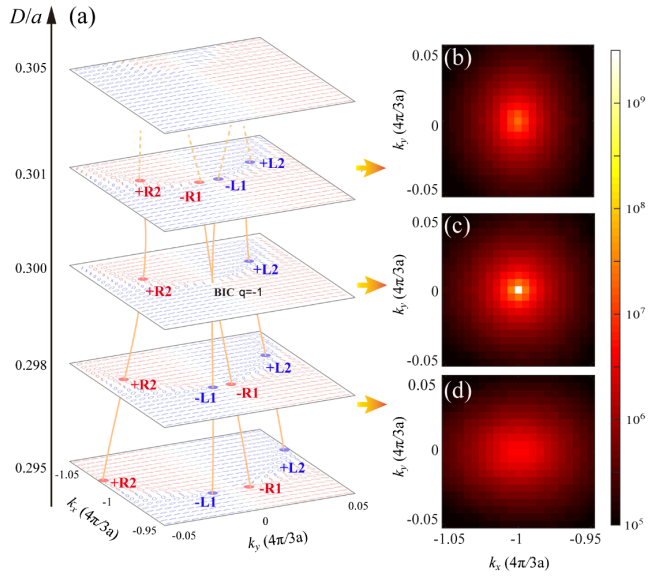

FIG. 3. Evolutions of C points and a BIC on the band of PhCSs near the K_1 point with varying diameters D and the fixed thickness h of $0.9074a$ (a). Here, the red (blue) disc denoted by $\pm Rn$ ($\pm Ln$) is a right- (left-) handed C point with a topological charge of $\pm 1/2$. Index n is used to denote different pairs of C points. The word "BIC" shows the position of the K-point BIC with a topological charge of $q = -1$ in Fig. 2(a). (b), (c),(d) Distributions of Q values of eigenmodes supported by the PhCSs with D equal to $0.301a$, $0.300a$, and $0.298a$ near the K-point BIC [Fig. 2(a)], respectively.

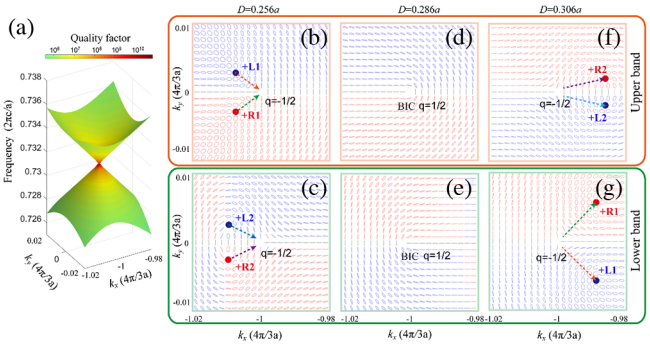

FIG. 4. Evolutions of C points and a double-degenerate BIC on two bands of the PhCS with Dirac cone dispersion. (a) Band structure of the PhCS with (D, h) equal to ($0.286a$, $1.036a$) supporting a Dirac-degenerate BIC at the K_1 point. The color hues represent Q values of eigenmodes. (b),(d), and (f) Far-field polarization states of eigenmodes in the upper band of PhCSs with the identical $h = 1.036a$ and increasing $D = 0.256a$ (b), $0.286a$ (d), and $0.306a$ (f), respectively. (c),(e) and (g) Far-field polarization states of eigenmodes in the lower band corresponding to (b), (d), and (f).

outwards and cross each other at the K_1 point. Here, the BIC with an infinite Q value appears [Figs. 3(b)–3(d)]. Meanwhile, another pair of C points outside the FBZ [shown in Fig. 2(a) with the topological charge of $1/2$ and denoted by $+R2/+L2$ in Fig. 3(a)] move inwards. These two pairs of C points with identical handedness and opposite charges are annihilated with each other when D reaches $0.305a$. The disappearance of polarization singularities is consistent with the sum of the topological charges equal to zero [Fig. 3(a)].

Furthermore, we study the behaviors of Dirac-degenerate BICS. The PhCS shown in Fig. 1(a) with $D = 0.286a$ and $h = 1.036a$ supports a TE-like double-degenerate BIC at the K_1 point with a real normalized frequency of 0.7311, where two TE-like bands of the PhCS linearly cross each other and form the Dirac cone dispersion [Fig. 4(a)] (for the detailed band structures, see Fig. s6 in Supplemental Material [24]). Figure 4(d) displays the far-field polarization states of eigenmodes in the upper band of the Dirac cone. Because of the y-mirror symmetry of the PhCS and the undefined polarization states of double-degenerate modes at the K_1 point, the far fields of eigenmodes with Bloch wave number $k_y = 0$ are TM and TE polarization on the left and right sides of the K_1 point, respectively. Based on Eq. (1), we can obtain that the topological charge carried by the Dirac-degenerate BIC is $1/2$. Figure 4(e) presents similar results of the eigenmodes in the lower band. Since the Dirac cone dispersion and double-degenerate modes at the K_1 point are protected by the spatial symmetry of the honeycomb-lattice PhCSs, when varying the diameter D of cylindrical holes etched in the PhCSs, the double-degenerate point is preserved at the K_1 point. But, it is not a BIC now. Figures 4(b) and 4(c) [4(f) and 4(g)], respectively, show the far-field polarization states of eigenmodes in the upper and lower band of the Dirac cone when the diameter D decreased (increased) to $0.256a$ ($0.306a$). Here, the topological charge carried by the Dirac-degenerate point at the K_1 point is $-1/2$, which is opposite to the Dirac-degenerate BIC [Figs. 4(d) and 4(e)]. The increased (reduced) topological charges originate from the merged (spawned) two pairs of C points carried the identical topological charges of $1/2$ at the K_1 point. When D is equal to $0.256a$, the two pairs of C points are outside the FBZ, denoted by $+R1/+L1$ in the upper band [Fig. 4(b)] and $+R2/+L2$ in the lower band [Fig 4(c)], respectively. Continuously increasing D, the two pairs of C points move inwards and cross each other at the K_1 point into the FBZ. The pair of C points denoted by $+R1/+L1$ ($+R2/+L2$) enters the lower (upper) band in Fig. 4(g) [Fig. 4(f)] [for details of the distributions of quality factors (Q value) of the eigenmodes, see Fig. s7 in Supplemental Material [24]).

In conclusion, focusing on polarization singularities near the boundary of the first Brillouin zone, we have theoretically demonstrated that the robust existence of the C point above the light line and the coexistence of different types of singular points of polarizations in the momentum space. Only a pair of C points with identical handedness and opposite topological charge can be annihilated together. It leads to diverse polarization states in the far-field

radiations of photonic crystal slabs (e.g., circular polarization, elliptical and linear polarizations with variant orientations). Distinct from the reported robust BICs inside the FBZ [12], the emergence of a BIC at the corner of FBZ just results from merging a pair of C points with identical topological charge and opposite handedness. Continuously varying the geometric parameters of PhCSs without breaking their spatial symmetry, the BIC could split into C points again. Interestingly, the topological charge carried by a Dirac-degenerate BIC (equal to $1/2$) is found to be opposite to that of a Dirac-degenerate point, because the interconversion between them is realized by the generation or annihilation of two pairs of C points with identical topological charges. The polarization diversity and the topological natures of different types of polarization singularities may open new directions for the study of topological photonic effects in the momentum space, and bring about new opportunities to generate and manipulate vector beams with diverse polarization states and different topological natures.

We are grateful to Professor Shuang Zhang and Dr. Biao Yang for fruitful discussions. The work was supported by the National Science Foundation of China (11974428, 61307072, 61405056).

*wmye72@126.com
†liujl@hit.edu.cn

[1] J. F. Nye, Lines of circular polarization in electromagnetic wave fields, Proc. R. Soc. A **389**, 279 (1983).
[2] M. V. Berry and M. R. Dennis, Polarization singularities in isotropic random vector waves, Proc. R. Soc. A **457**, 141 (2001).
[3] M. R. Dennis, Polarization singularities in paraxial vector fields: Morphology and statistics, Opt. Commun. **213**, 201 (2002).
[4] I. Freund, Polarization singularity indices in Gaussian laser beams, Opt. Commun. **201**, 251 (2002).
[5] J. D. Joannopoulos, S. G. Johnson, J. N. Winn, and R. D. Meade, *Photonic Crystals: Molding the Flow of Light*, 2nd ed. (Princeton University Press, Princeton, NJ, 2008).
[6] K. Sakoda, *Optical Properties of Photonic Crystals*, 2nd ed. (Springer, Berlin, 2005).
[7] D. C. Marinica, A. G. Borisov, and S. V. Shabanov, Bound States in the Continuum in Photonics, Phys. Rev. Lett. **100**, 183902 (2008).
[8] J. Lee, B. Zhen, S.-L. Chua, W. Qiu, J. D. Joannopoulos, M. Soljačić, and O. Shapira, Observation and Differentiation of Unique High-Q Optical Resonances Near Zero Wave Vector in Macroscopic Photonic Crystal Slabs, Phys. Rev. Lett. **109**, 067401 (2012).
[9] C. W. Hsu, B. Zhen, J. Lee, S.-L. Chua, S. G. Johnson, J. D. Joannopoulos, and M. Soljačić, Observation of trapped light within the radiation continuum, Nature (London) **499**, 188 (2013).
[10] R. Gansch, S. Kalchmair, P. Genevet, T. Zederbauer, H. Detz, A. M. Andrews, W. Schrenk, F. Capasso, M. Lončar, and G. Strasser, Measurement of bound states in the continuum by a detector embedded in a photonic crystal, Light Sci. Appl. **5**, e16147 (2016).
[11] C. W. Hsu, B. Zhen, A. D. Stone, J. D. Joannopoulos, and M. Soljačić, Bound states in the continuum, Nat. Rev. Mater. **1**, 16048 (2016).
[12] B. Zhen, C. W. Hsu, L. Lu, A. D. Stone, and M. Soljačić, Topological Nature of Optical Bound States in the Continuum, Phys. Rev. Lett. **113**, 257401 (2014).
[13] H. M. Doeleman, F. Monticone, W. d. Hollander, A. Alù, and A. F. Koenderink, Experimental observation of a polarization vortex at an optical bound state in the continuum, Nat. Photonics **12**, 397 (2018).
[14] Y. Zhang, A. Chen, W. Liu, C. W. Hsu, B. Wang, F. Guan, X. Liu, L. Shi, L. Lu, and J. Zi, Observation of Polarization Vortices in Momentum Space, Phys. Rev. Lett. **120**, 186103 (2018).
[15] B. Bahari, F. Vallini, T. Lepetit, R. Tellez-Limon, J. H. Park, A. Kodigala, Y. Fainman, and B. Kanté, Integrated and steerable vortex lasers, arXiv:1707.00181.
[16] J. Jin, X. Yin, L. Ni, M. Soljačić, B. Zhen, and C. Peng, Topologically enabled ultrahigh-Q guided resonances robust to out-of-plane scattering, Nature (London) **574**, 501 (2019).
[17] W. Liu, B. Wang, Y. Zhang, J. Wang, M. Zhao, F. Guan, X. Liu, L. Shi, and J. Zi, Circularly Polarized States Spawning from Bound States in the Continuum, Phys. Rev. Lett. **123**, 116104 (2019).
[18] A. Kodigala, T. Lepetit, Q. Gu, B. Bahari, Y. Fainman, and B. Kanté, Lasing action from photonic bound states in continuum, Nature (London) **541**, 196 (2017).
[19] A. Chen, W. Liu, Y. Zhang, B. Wang, X. Liu, L. Shi, L. Lu, and J. Zi, Observing vortex polarization singularities at optical band degeneracies, Phys. Rev. B **99**, 180101(R) (2019).
[20] T. Jacqmin, I. Carusotto, I. Sagnes, M. Abbarchi, D. D. Solnyshkov, G. Malpuech, E. Galopin, A. Lemaître, J. Bloch, and A. Amo, Direct Observation of Dirac Cones and a Flatband in a Honeycomb Lattice for Polaritons, Phys. Rev. Lett. **112**, 116402 (2014).
[21] J.-L. Liu, W.-M. Ye, and S. Zhang, Pseudospin-induced chirality with staggered optical graphene, Light Sci. Appl. **5**, e16094 (2016).
[22] J.-W. Dong, X.-D. Chen, H. Zhu, Y. Wang, and X. Zhang, Valley photonic crystals for control of spin and topology, Nat. Mater. **16**, 298 (2017).
[23] T. Ozawa, H. M. Price, A. Amo, N. Goldman, M. Hafezi, L. Lu, M. C. Rechtsman, D. Schuster, J. Simon, O. Zilberberg, and I. Carusotto, Topological photonics, Rev. Mod. Phys. **91**, 015006 (2019).
[24] See Supplemental Material at http://link.aps.org/supplemental/10.1103/PhysRevLett.124.153904 for the details of the band structures (note 1), the method used to obtain polarization states (note 2), the realizations of both C points and the K-point BIC by the interferences among multiple radiation channels (note 3), Fig. 2(a) in the main text (note 4), the projected trajectories of Figs. 2(b)–2(d), Supplemental Figs. s6 and s7 (Note 5).
[25] W. Ye, X. Yuan, C. Guo, J. Zhang, B. Yang, and S. Zhang, Large Chiroptical Effects in Planar Chiral Metamaterials, Phys. Rev. Appl **7**, 054003 (2017).